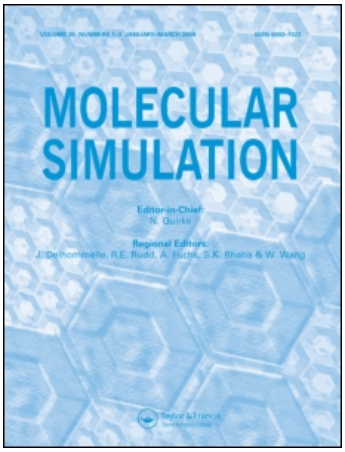

Molecular Simulation

Publication details, including instructions for authors and subscription information:
http://www.informaworld.com/smpp/title~content=t713644482

Molecular Simulation for Nanotechnologies: Application to Industry

Yasuaki Hiwatari[a]; Yutaka Kaneko[b]; Hiroaki Ishida[c]
[a] Department of Computational Science, Faculty of Science, Kanazawa University, Ishikawa, Japan [b] Department of Applied Analysis and Complex Dynamical Systems, Graduate School of Informatics, Kyoto University, Kyoto, Japan [c] Department of Mechanical Engineering, Ishikawa National College of Technology, Ishikawa, Japan

To cite this Article Hiwatari, Yasuaki , Kaneko, Yutaka and Ishida, Hiroaki(2004) 'Molecular Simulation for Nanotechnologies: Application to Industry', Molecular Simulation, 30: 13, 819 — 826
To link to this Article: DOI: 10.1080/08927020412331324658
URL: http://dx.doi.org/10.1080/08927020412331324658

Molecular Simulation, VOL. 30 (13–15), 15 November–30 December 2004, pp. 819–826

Taylor & Francis
Taylor & Francis Group

Molecular Simulation for Nanotechnologies: Application to Industry

YASUAKI HIWATARI[a,*], YUTAKA KANEKO[b] and HIROAKI ISHIDA[c]

[a]*Department of Computational Science, Faculty of Science, Kanazawa University, Kakuma, Ishikawa, 920-1192, Japan;* [b]*Department of Applied Analysis and Complex Dynamical Systems, Graduate School of Informatics, Kyoto University, Yoshida Hon-machi, Sakyo-ku, Kyoto 606-8501, Japan;* [c]*Department of Mechanical Engineering, Ishikawa National College of Technology, Tsubata, Ishikawa, 929-0392, Japan*

(Received February 2004; In final form October 2004)

In this plenary talk we will give examples of molecular simulations carried by us in relation to the nanotechnology and application to industrial problems in collaboration with industry people. This is the point of the presentation that can demonstrate the possibility of molecular simulations to solve real problems existing in industries. Here are two topics exhibited, electrodeposition in nano-scales and martensite transformation, which are essentially independent to each other, but it turns out that these molecular simulations work quite well. The electrodeposition involves a number of complex processes which take place near the interface between the solution and the solid substrate, which are not only classical dynamics in motions of particles, but also the quantum mechanical process like the exchange of electrons in adsorption and evaporation of metal atoms and metal ions. Here we are trying to develop a coarse-grained, or smart, model to examine large-scale phenomena. In the second part we will examine for the first time how the atomistic model can be predictable the martensite transformation in bulk. This is a typical case, in which many-body interactions are essential, and depends pretty much on the boundary condition, i.e. free boundary or periodic boundary. For the free-boundary condition the martensite transformation is rather easy to predict, while for the periodic-boundary condition it has never successfully been obtained so far using molecular dynamics (MD) simulation. Below we will discuss about these two topics separately.

Keywords: Electrodeposition; Kinetic Monte Carlo method; Damascene plating; Martensitic transformations; Molecular dynamics simulation; Modified embedded atom method; NiAl alloy

MOLECULAR SIMULATION OF ELECTRODEPOSITION

Electrodeposition is an important technique to plate thin film on metal surfaces by reduction reaction from electrolytic solutions, which has been widely used in many fields of electrochemical engineering[1]. Electrodeposition is a complicated process including both physical and chemical processes such as diffusion of solvated ions in solution, desolvation (dehydration) and reduction reaction followed by the diffusion of adatoms on the surface and crystallization. Recently electrodeposition has attracted great attention in semiconductor industries as a new tool to produce LSI interconnections. The IBM's group proposed a *dual damascene plating*, which is a replacement of the conventional vapor deposition of aluminum with electroplating copper[2]. In this method the lines (trenches) and via holes for three-dimensional electronic circuits are filled with copper by using electrodeposition technique. An important requirement for the success of this new method is to find out the optimal condition of electrodeposition, i.e. solution composition, additives, overpotential, etc. to fill trenches and via holes completely without creating any voids nor defects. Since the line width of recent LSI circuits is as small as microns or even of shorter scale, it is wrothwhile to understand the mechanism of copper deposition on an atomic length scale. Although advanced experimental techniques such as scanning tunneling microscope (STM) and atomic force microscope (AFM) have been developed to analyze the resulting surface structures on an atomic length scale, the behavior of ions and additives in solution during the deposition reactions is hard to be observed directly in experiments. Since the molecular simulation is a powerful tool to analyze the microscopic behavior of ions, substrate metals and additives, it would be desirable to develop

*Corresponding author. E-mail: hiwatari@cphys.s.kanazawa-u.ac.jp

ISSN 0892-7022 print/ISSN 1029-0435 online © 2004 Taylor & Francis Ltd
DOI: 10.1080/08927020412331324658

a method to deal with the metal deposition accompanying chemical reactions within the framework of molecular simulations.

The purpose of our study is to develop a new method for the simulation of electrodeposition and to apply it to electroplating technology to solve the problems which cannot be dealt with in experiments. In the following, we describe the kinetic Monte Carlo (MC) simulations of the solid-by-solid (SBS) model for electrodeposition and its application to damascene plating for LSI interconnections.

Kinetic Monte Carlo Simulation of Solid-by-solid Model

The SBS model is an extension of the Solid-on-Solid model for crystal growth to include the formation of vacancies during the surface growth. The system is a two- and three-dimensional square lattice each site of which represents either a solid atom, a liquid atom or a vacancy. Three reactions are taken into account: adsorption, desorption and the diffusion of surface atoms. When adsorption occurs, one of the liquid atoms adjacent to the surface solid atoms changes to a solid atom. The desorption is the reverse process. The rate constants for adsorption k_n^+, desorption k_n and surface diffusion k_{nm} depend upon the number of bonds n,m at each site. Following relations are assumed for the rate constants[3].

$$k_n/k_n^+ = \exp\{(n_k - n)\psi/k_BT - \mu/k_BT\}, \quad (1)$$

$$k_{nm} = (k_n k_m^+/k_1^+)\exp\{(\psi - E_d)/k_BT\}, \quad (2)$$

where ψ is the binding energy between atoms, μ the chemical potential and E_d the activation energy for the surface diffusion. The number of bonds at a kink site is denoted by n_k ($n_k = 2$ in two dimension and 3 in three dimension); μ is the control parameter of the growth, corresponding to the overpotential in electrodeposition. The kinetic MC simulation is performed using the algorithm of Bortz *et al.*[4]. The surface has a layer structure when μ is small and it becomes rough as μ increases. The basic properties of the SBS model are reported in our previous papers[5–7].

Three-dimensional SBS Model for Damascene Plating

As an application to the three-dimensional damascene plating, we performed the kinetic MC simulation of filling a via hole and a trench using the SBS model. The parameters are $\psi/k_BT = 11.5$, $\mu/k_BT = 20$ and $E_d = \psi/2$. Figure 1(a) shows the initial surface of the simulation of via-filling. The diameter of the hole is 30 lattice sites and the aspect ratio is 2. The periodic boundary condition is assumed in x- and y-directions. Figure 1(b) is the surface structure and the voids in the film after the filling. It is observed that large voids elongated in z-direction are observed in the middle of the hole. The filling is far less complete although the final surface is almost flat. Figure 2 shows the results of filling a trench using the same parameters. The width of the trench is 30 lattice sites and the aspect ratio is 2. In this case voids appear in the middle of the trench, which are formed when some parts of the surfaces from two sides meet during the simulation. The qualitative features of the voids are similar to those found in experiments although the size of the simulation system is smaller than experiments[8].

The SBS Model with Additives

A small amount of additives in solution are important in electrodepostion to control the local overpotential and the surface structure. Various kinds of additives have been investigated, which are used as levelers, brighteners, and so on. In the case of copper plating, three kinds of additives are commonly used: polyethylene glycol (PEG), bis (3-sulfopropyl) disulfidedisodium (SPS) and Janus Green B (JGB), which are known as inhibitors, accelerators and levelers, respectively.[8,9] PEG and JGB have the effect

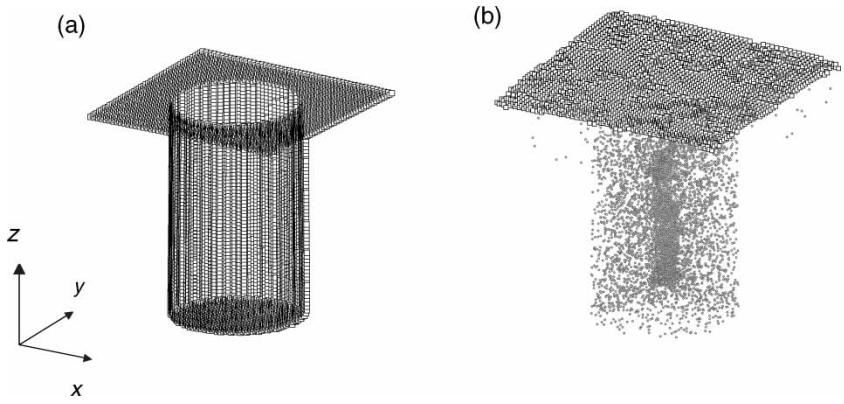

FIGURE 1 (a) Initial surface for the simulation of filling a via hole. (b) Results of the kinetic MC simulation. Small squares show the final surface structure and dots denote vacancies.

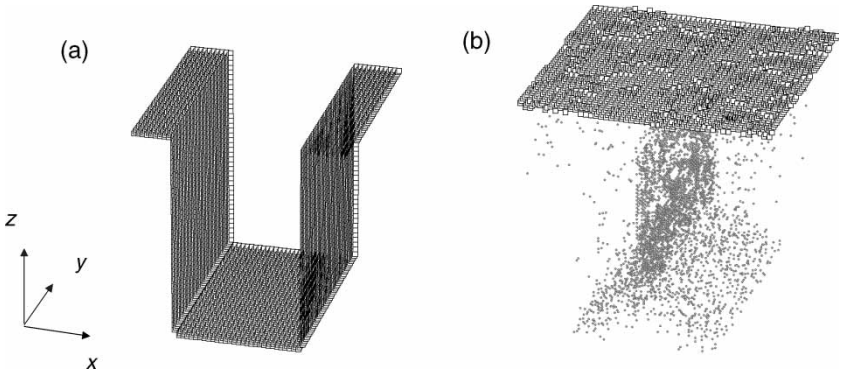

FIGURE 2 (a) Initial surface for the simulation of filling a trench. (b) Results of the kinetic MC simulation. Small squares show the final surface structure and dots denote vacancies.

of preventing the adsorption of new atoms on the surface, while SPS is an accelerator which increases the local growth rate. In this paper, we include additives in the two-dimensional SBS model to find the condition to eliminate the void formation. The additives are assumed to be inhibitors. They occupy the lattice sites in the solution part of the model and move to the surface by random walk. The surface growth of the SBS model and the random walk of additives are simulated simultaneously. When the additives reach the surface, the local growth rate on the surface sites within a certain range from the additives is reduced. The range of this inhibiting effect is regarded as the size of the additives. Additives are assumed to stick to the surface with a probability k_{ad}.

Figures 3 (a)–(c) show the results of via filling with and without additives. The initial surface has a rectangular hole the aspect ratio of which is 2. The width of the hole is 100 lattice sites and the parameters for the SBS model are $\psi/k_BT = 9.44$, $\mu/k_BT = 10.0$ and $E_d = \psi/2$. Figure 3 (a) shows the film structure generated by the simulation without additives. Large voids elongated in the growth direction appear in the hole, which are similar to those found in the three-dimensional model. The results with additives are shown in Fig. 3(c) with the distribution of the additives in Fig. 3(b). The concentration of the additives is 0.13% and the inhibiting range is 4 lattice spacing. It is clearly observed that the additives are distributed around the upper part of the hole, reducing the growth rate of the upper surface. Some of the additives are embedded in the film. As a result, the void size in the middle of the hole becomes small compared to the case without additives. Such an effect of inhibitors is in agreement with those found in experiments.[8,9] Although the void size is reduced compared to the additive-free case, the effect of inhibitors is not enough for eliminating voids completely. In experiments, the combination of three kinds of additives mentioned above is investigated to establish the bottom-up process and the superconformal filling. We are now trying to include accelerators as well as inhibitors in the SBS model. The results of the simulations with two kinds of additives are reported in a separate paper of this issue.

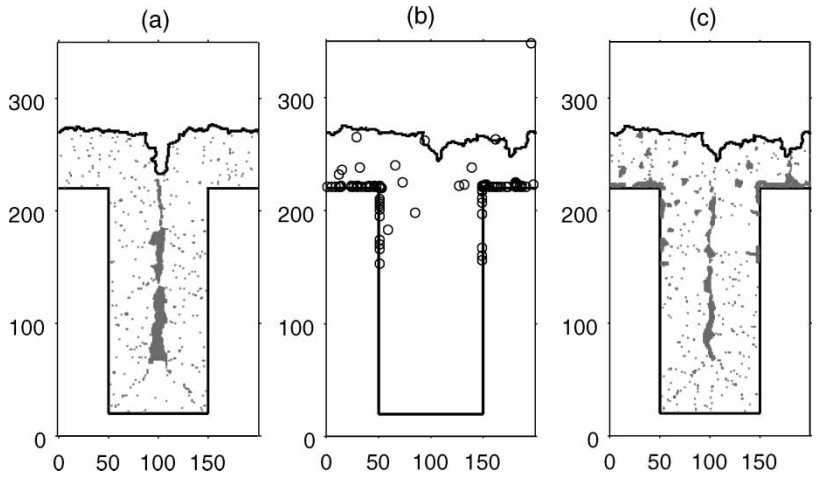

FIGURE 3 Results of the two-dimentional simulation of filling a hole. (a) Film structure generated by the simulation without additives. Dots denote vacancies. (b) Distribution of additives. (open circles) (c) Film structure generated by the simulation with additives. The labels denote the number of lattice sites.

Summary

In the SBS model, the parameters characterizing the additives such as the range of inhibition are input parameters for the simulation. It would be desirable to decide these parameters within the framework of the simulations. For that purpose, we have developed a hybrid method of MD and MC for the molecular simulation of electrodeposition. In this method, we solve the equations of motion of all the particles in the system of solution–electrode interface by the MD method, while the deposition reaction on the electrode surface is realized by the MC method[10]. We expect that the combined system of the MD–MC hybrid method (to get microscopic information) and the SBS model (to perform large scale simulations) would be the tool of the molecular simulation for the nano-scale electroplating technology. Since the optimal condition for the additives are investigated by trial and error procedure in most of the experiments, the number of trial experiments will be reduced greatly if the ranges of parameters are estimated by the molecular simulations.

MARTENSITIC TRANSFORMATIONS IN NiAl ALLOY

To take into account many-atom effects for metals and alloys, the embedded atom method (EAM) [11,12] has been used for the present study of metals and alloys.

The EAM based on the density-functional theory has been successfully applied to the fcc or nearly filled *d*-band transition metals, and it has been quite successful in predicting numerous properties of metals and alloys. However, with the spherically averaged electron density, which therefore precludes directional bonding, applications to other metals are restricted.

Recently, the modified embedded atom method (MEAM) which takes into account the screening effect of the interatomic interactions and angular dependence has been developed[13–16]. In the EAM, the electron density is a simple sum of radically dependent contributions from other atoms, while the MEAM takes into account the angular dependence of the electron density. Also, the MEAM incorporates a strong screening function so that interactions can be very short ranged for atoms, which are reasonably tight packed, but can be long ranged in open conditions such as atoms in surface. The MEAM has been successfully extended to the study of mechanical properties of fcc, bcc, hcp and diamond cubic crystal structures.

Martensitic transformations have been studied [17,18] using the EAM potentials [19,20] with computational methods and respective boundary conditions: A rectangular computational crystal with free surface boundary conditions to the x and y directions and the periodic boundary condition along the z direction, or a cylindrical crystal with free surface boundary conditions to x and y directions and the periodic boundary condition to the z direction and with a small-angle tilt grain boundary [18], or crack-displacements in an anisotropic crystal[17]. The martensitic transformation is a first-order, displacive (displacements of atoms being much less than the atomic spacing) and diffusionless transition. In NiAl alloy, the high-temperature crystal structure called parent phase is CsCl type B2 (ordered bcc structure), and the low-temperature crystal structure called martensitic phase is 3R (the stacking in $(110)_{B2}$ plane is ABCABC…). The martensitic transformation in NiAl is a thermoelastic type transformation accompanied by a temperature hysteresis (a few to several tens of degree), a mobile twin interface and a crystallographically reversible transformation.

For the martensitic transformation shear strains play an important role. Nucleation and its growth characterize the nature of the transformation because of the first-order transition. However, for example the mechanisms of the transition as well as atomic displacements in the nucleation process are not well understood.

The purpose of the present work is to carry out MD simulations of the martensitic transformations in NiAl alloy with a bulk (no surface) computational model using the MEAM potentials so as to find these properties and construct a microscopic model for the martensitic transformations.

COMPUTATIONAL PROCEDURE

Interaction Potentials

Within the framework of the EAM [11,12] and MEAM [13–16] the total energy E_{tot} of the system containing N atoms is represented by

$$E_{\mathrm{tot}} = \sum_{i=1}^{N} \left[F_i(\bar{\rho}_i) + \frac{1}{2} \sum_{j \neq i}^{N} \phi_{ij}(r_{ij}) \right], \tag{3}$$

where F_i is the embedding function for the type-i atom, $\bar{\rho}_i$ the background electron density at site i, ϕ_{ij} (r_{ij}) a pair potential between site i and site j atoms separated by the distance r_{ij}. In the EAM, $\bar{\rho}_i$ is given by a linear superposition of spherically averaged atomic electron densities, while in the MEAM, $\bar{\rho}_i$ is augmented by angular dependent terms.

The energy per atom in the reference structure for the alloy system is given by a universal energy function [21]

$$E_{ij}^{u}(r_{ij}) = -E_{ij}^{0}\left[1+\alpha_{ij}\left(\frac{r_{ij}}{r_{ij}^{0}}-1\right)\right]\exp\left[-\alpha_{ij}\left(\frac{r_{ij}}{r_{ij}^{0}}-1\right)\right],$$

$$\alpha_i = \sqrt{\frac{9B_i\Omega_i}{E_i^0}}, \tag{4}$$

where B_i is the bulk modulus, Ω_i the atomic volume of the solid materials and E_i^0 the cohesive energy, which are all evaluated at equilibrium in the reference structure for the type-i atom. $E_{ij}^0 = (E_i^0 + E_j^0)/2 - \Delta_{ij}$, where Δ_{ij} is the enthalpy of mixing the type-i and type-j atoms, $\alpha_{ij} = (\alpha_i + \alpha_j)/2$, r_{ij}^0 calculated from the summed equilibrium intermetallic atomic volumes $\Omega_{ij} = (\Omega_i + \Omega_j)/2$.

Many-body screening function S_{ik} that quantifies the screening between two atoms site i and site k due to other atoms in the system, say site j. Both the atomic electron densities and the pair potentials are multiplied by this function. If the atoms are unscreened, $S_{ik} = 1$ and if they are completely screened, $S_{ik} = 0$. The screening function depends on the configurations of all atoms in the system,

$$S_{ik} = \prod_{j\neq i,k} S_{ijk} \tag{5}$$

S_{ijk} is calculated using a simple geometric construction. Consider an ellipse passing through atoms sites i, j, and k with the minor axis of the ellipse determined by atoms site i and site k. The equation of the ellipse is given by

$$x^2 + \frac{1}{C}y^2 = \left(\frac{r_{ik}}{2}\right)^2,$$
$$C = \frac{2(X_{ij}+X_{jk}) - (X_{ij}+X_{jk})^2 - 1}{1-(X_{ij}+X_{jk})^2}, \tag{6}$$

where $X_{ij} = (r_{ij}/r_{ik})^2$ and $X_{jk} = (r_{jk}/r_{ik})^2$. The r's are the distance between the respective atoms. We assume a smooth function of C,

$$S_{ijk} = f_c\left(\frac{C - C_{\min}}{C_{\max} - C_{\min}}\right), \tag{7}$$

where $C_{\min}$ and $C_{\max}$ are two limiting values of C. The smooth cut-off function $f_c(x)$ is defined [15] as

$$f_c(x) = \begin{cases} 1 & 1 \le x \\ \{1-(1-x)^4\}^2 & 0 < x < 1 \\ 0 & x \le 0 \end{cases} \tag{8}$$

Computational Methods

The martensitic transformation temperature of NiAl varies very rapidly with composition in the range 60–66 at.%Ni[22]. The transformation temperature of $Ni_{0.625}Al_{0.375}$ alloy is around the room temperature which is useful for the functionality material.

We performed MD simulations with the MEAM potentials for the $Ni_{0.625}Al_{0.375}$ alloy using the Gear algorithm, time step $\Delta t(= 1\,\text{fs})$ and the three-dimensional-periodic-boundary conditions.

The MEAM parameters (the sublimation energy E_i^0, the equilibrium nearest-neighbor distance r_i^0, the exponential decay factor for the universal energy function α_i, the scaling factor for the embedding energy A_i, the exponential decay factors for the atomic densities $\beta_i^{(l)}$ and the weighting factors for the atomic densities $t_i^{(l)}$) for NiAl alloy are the same as our previous work[23]. The enthalpy of mixing for Ni and Al Δ_{ij} [14] is taken to be -0.48 eV per atom.

The limiting value $C_{\max} = 2.8$ is assumed to be a little bit smaller than 3 so that the nearest neighbor atoms in the fcc structure ($C = 3$ for $r_{ik} : r_{ij} : r_{jk} = 1:1:1$ from Eq. (6)) are unscreened in consideration of the thermal vibration. On the other hand, $C_{\min} = 2.0$ is the threshold value that the second neighbor atoms in the bcc structure ($C = 2$ for $r_{ik} : r_{ij} : r_{jk} = 1 : \sqrt{3}/2 : \sqrt{3}/2$) are just screened. Therefore, the influence of the thermal vibration on the second neighbor atoms in the bcc structure appears a little greatly for the phase transformation between B2 (ordered bcc structure) and 3R (stacking fcc in $(110)_{B2}$ plane is ABCABC...) in NiAl alloy. $C_{\min}$ was altered into 2.35 from the original [14] value 2.0 to avoid this difficulty. By this change, the transformation temperature fell down and not only the transformation but also that reverse transformation have been obtained.

In the present MD simulation the pressure of the system was controlled by the Parrinello-Rahman scheme with the external pressure $P_{\text{ext}} = 0$ and the external stress $S_{\text{ext}} = 0$. The temperature was controlled by the Nosé-Hoover method. MD simulations were started with a given initial structure and temperature with initial random velocities following the Boltzmann distribution. The total number of atoms N is 432 for the present MD system of NiAl. The initial configuration was set with the B2 or 3R structure to satisfy the composition of the respective atoms, Ni and Al, which are randomly distributed. The equilibrium nearest-neighbor distance $r_{ij}^0 = \Omega_{ij}^{1/3}$ is calculated from the summed equilibrium intermetallic atomic volumes Ω_{ij} for NiAl.

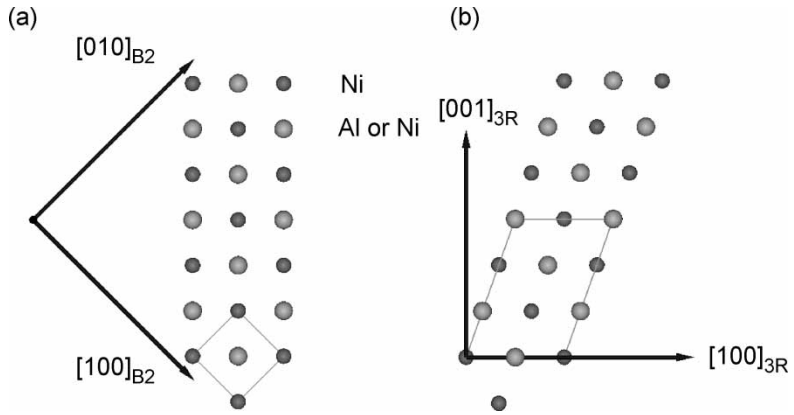

FIGURE 4 The relationship of the crystallographic orientations for NiAl between (a) B2 and (b) 3R structures. The thin solid lines show a unit cell in each structure.

RESULTS AND DISCUSSIONS

Martensitic Transformation by Continuous Cooling and Heating Processes

Starting with an initial state of B2 structure as a parent phase for $Ni_{0.625}Al_{0.375}$ alloy, the temperature was decreased from 1000 to 100K at the rate of 0.01K/step, and increased from 100 to 1000K at the same rate.

The orientational relationship of B2 (ordered bcc structure) and 3R (stacking fcc in $(110)_{B2}$ plane is ABCABC...) structure for NiAl is shown in Fig. 4.

The time dependence of three cell constants, h_{11}, h_{22} and h_{33} in this MD simulation is shown in Fig. 5. Three cell constants take similar values irrespective of both cooling and heating processes below 380K and above 780K. Between 380 and 780K they depend on either process, showing a hysteresis.

In these simulations, the thermally induced B2 to 3R structural change and the reverse transformation were obtained. It is observed in Fig. 5 that the martensite-start temperature upon cooling (M_s) is about 460K and the martensite-finish temperature upon cooling (M_f) is 380K, while the reverse martensite-start temperature upon heating (A_s) is about 750K and the reverse martensite-finish temperature upon heating (A_f) is 780K.

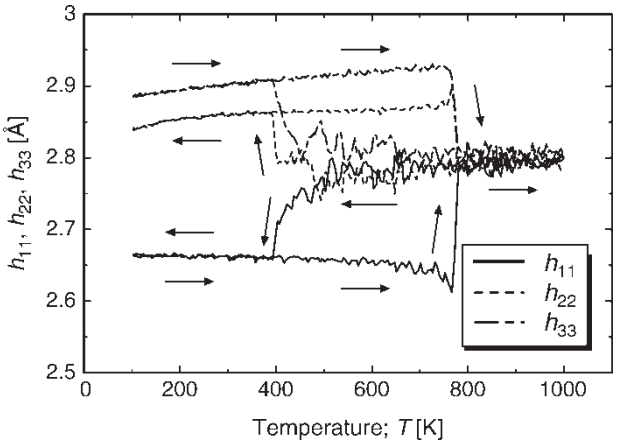

FIGURE 5 The temperature dependence of three cell constants for $Ni_{0.625}Al_{0.375}$ during the continuous cooling and heating process.

These transition hysteresis is significantly wider than experimental data which are in the range of several tens of degree[24,25]. In order to examine those discrepancies between MD results and experiments further considerations are needed, such as size effects of the MD calculation, effects of the periodic boundary conditions used and so on.

The orientational relationship of the atomic configuration, $(001)_{B2}\|(001)_{3R}$ and $[110]_{B2}\|[100]_{3R}$ are shown in Fig. 6. In 3R martensitic phase the ABCABC... stacking of $(110)_{B2}$ plane has been observed.

In Fig. 6 (a) the lattice-invariant deformation is shown in 3R structure at 100K for $Ni_{0.625}Al_{0.375}$. A twin is clearly seen in $(0\bar{1}0)$ plane. The 3R phase is accompanied by a twin which leads to a lattice-invariant deformation. In the 3R phase at $T = 100$K, the internal potential energy within the twin structure is -4.46 eV/atom on the other hand, it is -4.48 eV/atom without twin. The decrease of the internal potential energy leads to minimizing the transformation strain energy.

Concentration Dependence of the Transformation Temperature

The concentration dependence of the martensite-start temperature was studied by starting with an initial state of B2 structure as a parent phase for Ni_xAl_{1-x} $(0.58 < x < 0.69)$ alloy, the temperature was cooled from 1000 to 100K at the rate of 0.01K/step. The concentration dependence of the transformation temperature for $C_{min} = 2.0$ and 2.35 is shown in Fig. 7. The transformation temperature for $C_{min} = 2.35$ fell down in comparison with $C_{min} = 2.0$ and agrees with the experiments[22]. The sensitivity of the transformation temperature on

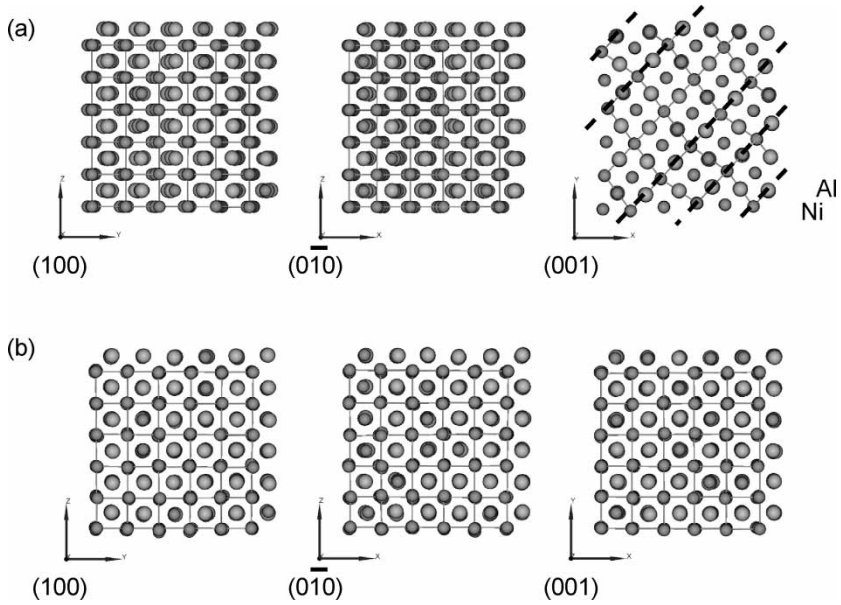

FIGURE 6 The lattice-invariant deformation in 3R structure at $T = 100$K for $Ni_{0.625}Al_{0.375}$ (a). For a comparison the B2 structure at $T = 1000$K is shown in (b). The thin solid lines show the unit cells in each structure and the dashed lines show the twin boundaries.

composition 35 K/at.%Ni for $C_{min} = 2.35$ is lower than the experimental value 170K/at.%Ni.

SUMMARY

The martensitic transformations in NiAl alloys were studied using molecular dynamics (MD) simulations. The modified embedded atom method was used with the pseudo monoatomic potentials in which the angular dependence was taken into consideration.

The following conclusions can be drawn. The thermally induced martensitic B2 → 3R transformations and the reverse 3R → B2 transformations have been obtained in the present MD simulations for the first time with a bulk (no surface) computational model. The transformation is accompanied by a twin in the 3R phase which leads to a lattice-invariant deformation so as to minimize the transformation strain energy.

The crystallographic orientation relationship, $(001)_{B2}\|(001)_{3R}$ and $[110]_{B2}\|[100]_{3R}$ was found, which agrees with experiments. The concentration dependence of the transformation temperature for Ni_xAl_{1-x} $(0.58 < x < 0.69)$ alloys has been observed.

The present MD simulation was carried with a medium-size of computational cell. The MEAM potentials are useful since they involve many-body effects through the electron density. In this respect large-scale MD simulations may be challenging to study phase transformations for bulk alloys of various kinds.

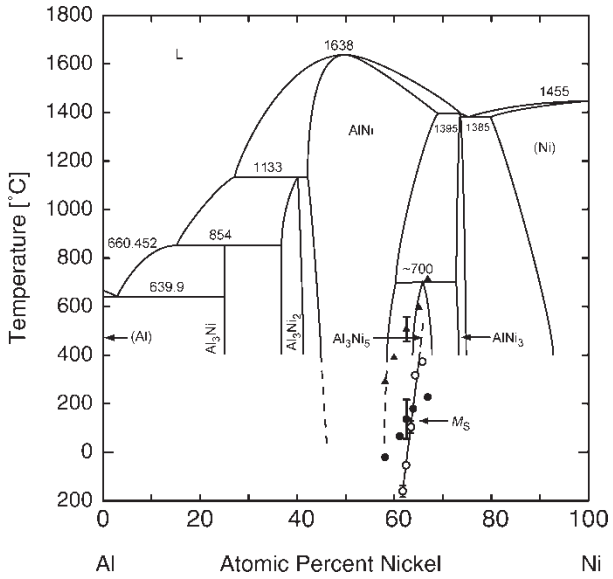

FIGURE 7 Assessed Ni—Al phase diagram from Ref. [26] The concentration dependence of the transformation temperature M_s is also reported: circles from Ref. [22] and dots ($C_{min} = 2.35$) and triangles ($C_{min} = 2.0$) from MD simulation of the present work.

References

[1] Bockris, J.O'M. and Reddy, A.K.N. (1998) *Modern Electrochemistry*, 2nd Ed. (Plenum Press, New York and London).
[2] Andricacos, P.C., Uzoh, C., Dukovic, J.O., Horkans, J. and Deligianni (1998) "Damascene copper electroplating for chip interconnections", *IBM J. Res. Dev.* **42**, 567.
[3] Gilmer, G.H. and Bennema, P. (1972) "Simulation of crystal growth with surface diffusion", *J. Appl. Phys.* **43**, 1347.
[4] Bortz, A.B., Kalos, M.H. and Lebowitz, J.L. (1975) "A new algorithm for Monte Carlo simulation of Ising spin systems", *J. Comput. Phys.* **17**, 10.
[5] Kaneko, Y., Hiwatari, Y., Ohara, K. and Murakami, T. (2000) "Monte Carlo simulation of thin film growth with lattice defects", *J. Phys. Soc. Jpn* **69**, 3607.
[6] Kaneko, Y. and Hiwatari, Y. (2002) "The solid-by-solid model for crystal growth and electroplating: Kinetic Monte Carlo simulation", *Recent Research Developments in*

Physics and Chemistry of Solids (Transworld Research Network), Vol. 1, p 48.
[7] Kaneko, Y., Hiwatari, Y., Ohara, K. and Murakami, T. (2003) "Computer simulation thin film growth with defect formation", *Surf. Coat. Tech.* **169–170**, 215.
[8] Moffat, T.P., Bonevich, J.E., Huber, W.H., Stanishevsky, A., Kelly, D.R., Stafford, G.R. and Josell, D. (2000) "Superconformal electrodeposition of copper in 500–900 nm features", *J. Electrochem. Soc.* **147**, 4524.
[9] Miura, S., Oyamada, K., Takada, Y. and Honma, H. (2001) "ULSI wiring formation by copper electroplating in the presence of additives", *Electrochem. Soc. Jpn* **69**, 773.
[10] Ueno, Y. (2002) "Molecular simulation of thin film growth with electrodeposition at solid–liquid interface" (Kyoto University).
[11] Daw, M.S. and Baskes, M.I. (1983) "Semiempirical quantum mechanical calculation of hydrogen embrittlement in metals", *Phys. Rev. Lett.* **50**, 1285–1288.
[12] Daw, M.S. and Baskes, M.I. (1984) "Embedded-atom method: Derivation and application to impurities, surfaces, and other defects in metals", *Phys. Rev. B* **29**, 6443.
[13] Baskes, M.I. (1987) "Application of the embedded-atom method to covalent materials: a semiempirical potential for silicon", *Phys. Rev. Lett.* **59**, 2666.
[14] Baskes, M.I. (1992) "Modified embedded-atom potentials for cubic materials and impurities", *Phys. Rev. B* **46**, 2727.
[15] Baskes, M.I. (1997) "Determination of modified embedded atom method parameters for nickel", *Mater. Chem. Phys.* **50**, 152.
[16] Baskes, M.I. (1999) "Atomistic potentials for the molybdenum-silicon system", *Mater. Sci. Eng. A* **261**, 165.
[17] Grujicic, M. and Dang, P. (1995) "Molecular Dynamics embedded atom method simulations of creak-up transformation toughening in Fe—Ni austenite", *Mat. Sci. Eng. A* **199**, 173.
[18] Grujicic, M. and Dang, P. (1995) "Computer simulation of martensitic transformation in Fe—Ni face-centered cubic alloys", *Mat. Sci. Eng. A* **201**, 194.
[19] Johnson, R.A. and Oh, D.J. (1989) "Analytic embedded-atom method for bcc metals", *J. Mater. Res.* **4**, 1195.
[20] Johnson, R.A. (1989) "Alloy models with the embedded-atom method", *Phys. Rev. B* **39**, 12554.
[21] Rose, J.H., Smith, J.R., Guninea, F. and Ferrante (1984) "Universal features of the equation of state of metals", *Phys. Rev. B* **29**, 2963.
[22] Au, Y.K. and Wayman, C.M. (1972) "Thermoelastic behavior of the martensitic transformation in β′ NiAl alloys", *Scr. Metall.* **6**, 1209.
[23] Ishida, H., Motoyama, S., Mae, K. and Hiwatari, Y. (2003) "Molecular dynamics simulation of martensitic transformations in NiAl alloy using the modified embedded atom method", *J. Phys. Soc. Jpn* **72**, 2539.
[24] Chakravorty, S. and Wayman, C.M. (1976) "The thermoelastic martensitic transformation in beta′ Ni—Al alloys I. crystallography and morphology", *Met. Trans. A* **7**, 555.
[25] Ochiai, S. and Ueno, M. (1988) "Composition dependence of the M_s temperature in the beta′ NiAl compound", *J. Jpn Inst. Met.* **52**, 157.
[26] Singleton, M.F., Murray, J.L. and Nash, P. (1986) In: Massalski, T.B., ed., *Binary Alloy Phase Diagrams* (American Society for Metals, Metals Park, OH).